

PROBABILISTIC CLASSIFICATION OF NEAR-SURFACE SHALLOW-WATER SEDIMENTS USING A PORTABLE FREE-FALL PENETROMETER

Md Rejwanur Rahman¹, Adrian Rodriguez-Marek, Ph.D², Nina Stark, Ph.D³, Grace Massey,
Ph.D⁴, Carl Friedrichs, Ph.D⁵, and Kelly M. Dorgan, Ph.D⁶

¹Charles E. Via, Jr. Department of Civil and Environmental Engineering, Virginia Tech, 750
Drillfield Dr., Blacksburg, VA 24060. E-mail: rejwan@vt.edu

²Charles E. Via, Jr. Department of Civil and Environmental Engineering, Virginia Tech, 750
Drillfield Dr., Blacksburg, VA 24060. E-mail: adrianm@vt.edu

³Engineering School of Sustainable Infrastructure and Environment (ESSIE), University of
Florida, Gainesville, FL 32611. E-mail: nina.stark@essie.ufl.edu

⁴Virginia Institute of Marine Science, William & Mary, Gloucester Point, VA 23062. E-mail:
grace.massey@vims.edu

⁵Virginia Institute of Marine Science, William & Mary, Gloucester Point, VA 23062. E-mail:
carl.friedrichs@vims.edu

⁶Dauphin Island Sea Lab, 101 Bienville Blvd., Dauphin Island, AL, 36528. E-mail:
kdorgan@disl.org

ABSTRACT

The geotechnical evaluation of seabed sediments is important for engineering projects and naval applications, offering valuable insights into sediment properties, behavior, and strength. Obtaining high-quality seabed samples can be a challenging task, making in-situ testing an essential part of site characterization. Free Fall Penetrometers (FFP) have emerged as robust tools for rapidly profiling seabed surface sediments, even in energetic nearshore or estuarine conditions and shallow

as well as deep depths. While methods for interpretation of traditional offshore Cone Penetration Testing (CPT) data are well-established, their adaptation to FFP data is still an area of research. In this study, we introduce an innovative approach that utilizes machine learning algorithms to create a sediment behavior classification system based on portable free fall penetrometer (PFFP) data. The proposed model leverages PFFP measurements obtained from locations such as Sequim Bay (Washington), the Potomac River, and the York River (Virginia). The result shows 91.1% accuracy in the class prediction, with the classes representing cohesionless sediment with little to no plasticity, cohesionless sediment with some plasticity, cohesive sediment with low plasticity, and cohesive sediment with high plasticity. The model prediction not only provides the predicted class but also yields an estimate of inherent uncertainty associated with the prediction, which can provide valuable insight about different sediment behaviors. These uncertainties typically range from very low to very high, with lower uncertainties being more common, but they can increase significantly depending on variations in sediment composition, environmental conditions, and operational techniques. By quantifying uncertainty, the model offers a more comprehensive and informed approach to sediment classification.

INTRODUCTION

The use of Free Fall Penetrometers is motivated by the need for rapid and quantitative geotechnical assessment of seabed sediments in a variety of engineering projects and naval applications. In-situ tests to obtain geotechnical properties represent an important offshore site investigation method due to the inherent challenges associated with collecting high-quality seabed samples in many environments. Free Fall Penetrometers (FFP) can swiftly profile the seabed's surface sediments, even in dynamic nearshore conditions and to depths ranging from several meters to over a thousand meters below the water's surface (Akal and Stoll 1995; Albatal and Stark 2017). FFP instruments collect data with a vertical resolution often better than 1 cm in the uppermost seabed layer. Moreover, they can be deployed in a cost- and time-efficient manner in settings characterized by energetic hydrodynamics and active sediment dynamics (Stark et al. 2012; Albatal et al. 2020). Datasets obtained from FFP tests have found applications in various domains. For instance,

Mulukutla et al. (2011) used FFP data to infer information about the grain size of the sediments. Aubeny and Shi (2006), followed by Chow et al. (2014) & Chow et al. (2017), estimated undrained shear strength based on FFP measurements in fine-grained sediments while Albatal et al. (2020) established correlations between FFP decelerations and relative density and explored diverse methods for estimating critical friction angles in coarse-grained sediments. Jaber and Stark (2023) introduced a framework to obtain geotechnical properties such as undrained shear strength or friction angle for any typical seabed sediment types.

Although a range of methodologies has been proposed for classifying data derived from traditional CPT, including deterministic and probabilistic approaches (Robertson 1990; Olsen and Mitchell 1995; Jung et al. 2008; Cetin and Ozan 2009), the application of probabilistic approaches to FFP data remains largely unexplored. The implementation of a probabilistic approach for FFP data could enable a sediment classification scheme to distinguish between different seabed geomechanical behavior. Hence, this study aims to address the following key questions:

1. How to develop a sediment behavior classification scheme using portable FFP (PFFP) data?
2. How to quantify associated uncertainties in sediment behavior classification?

This study proposes a predictive model based on machine learning. The model leverages PFFP measurements obtained from Sequim Bay (Washington) and the Potomac and York Rivers (Virginia). In this paper, we start by discussing the data collection procedure and corresponding lab testing. Then different technical components (i.e., model architecture, dataset processing and model training) of the proposed model are presented. Next, a step-by-step guide for predicting the sediment class using the proposed model is presented. Finally, the results of the model are presented and discussed along with some of the example prediction scenarios.

DATA COLLECTION

Deceleration, Velocity, and Penetration Depth

The PFFP used in this study is equipped with a set of five accelerometers designed to measure both vertical deceleration and tilt, allowing the derivation of vertical velocity and bed penetration

depth. These accelerometers possess varying measurement ranges, spanning from $\pm 2g$ to $\pm 250g$, with g denoting gravitational acceleration. The PFFP has dimensions of 63.1 cm in length, 8.75 cm in diameter, and weighs 7.7 kg when equipped with the 60° conical tip option. Several sources investigated the processing of accelerometer-based PFFP data, as documented in the works of Mulukutla et al. (2011), Albatal and Stark (2017), Mumtaz et al. (2018), Bilici et al. (2019), and Hunstein et al. (2023), to name just a few. By integrating deceleration data recorded during seabed penetration, the probe's velocity and depth of penetration is calculated. Figure 1(a) shows a PFFP deployment, while Figure 1(b) and 1(c) present PFFP sample data displaying the measured deceleration and derived penetration velocity against its displacement.

Survey Locations and Sediment Sampling

Surveys were conducted in three distinct locations: Sequim Bay, WA; Potomac River, VA; and York River, VA, between 2018 and 2022. The locations are shown in Figure 2, and a detailed distribution of the number of PFFP deployments among different locations is shown in Table 1. Along the York River estuary, deployments were divided into eight sub-locations. In total, 447 PFFP deployments were carried out in these three sites. In addition to PFFP testing, sediment samples and cores were collected using various techniques based on the specific sediment types and with the goal of retrieving high-quality seabed samples. For cohesive sediments, methods such as box coring and gravity coring were employed, while diver sampling was primarily used in sandy sediment areas, in addition to grab sampling.

Sediment Class Determination

The collected sediment samples were classified according to the Unified Soil Classification System (USCS) outlined in ASTM D2487 (ASTM 2017). This classification system considers particle size gradation and Atterberg limits, including the Plasticity Index and Liquid Limit. Based on the USCS classification, the sediments were categorized into four major types. Detailed information regarding these soil behavior types can be found in Table 2. The sand content (percentage of sediment with grain size larger than 0.075 mm) and fines content (percentage of sediment with grain size smaller than 0.075 mm) were determined in accordance with the specifications outlined

by the USCS (ASTM D2487). Classes 1 and 2 can be categorized as sandy sediments with a sand content exceeding 50%. The primary distinction between Class 1 and Class 2 is based on the fines content, which is set at 12% according to the Unified Soil Classification System (USCS). Similarly, Classes 3 and 4 are classified as fine-grained muddy sediments, characterized by a fines content greater than 50%. The key differentiating criterion between Class 3 and Class 4 is the liquid limit. It has been found that highly plastic minerals such as montmorillonite tend to have higher liquid limits than low plasticity minerals such as kaolinite (Mitchell and Soga 2005). Therefore, the liquid limit can be used as a proxy for determining plasticity of a sediment. The USCS distinguishes high and low plasticity of clay or silt by a threshold value of liquid limit equal to 50. The same criteria have been used here to distinguish between Class 3 and Class 4. The sediment class obtained from laboratory testing is then used to train the predictive model for connecting the PFFP data to the sediment classes. Among the four classes, Class 4 was identified as the most dominant, comprising a total of 267 data points. This was followed by Class 1 with 119 data points, Class 2 with 40 data points, and Class 3 with 23 data points. The issue of dataset imbalance is addressed later in this paper. The dataset employed in this study is depicted in Figure 3, mapped onto the space of maximum deceleration and penetration depth.

PROBABILISTIC PREDICTIVE MODEL

Here we use a probabilistic predictive model approach, which builds on previous work which utilized subsets of parameters obtained from the PFFP data. Jaber and Stark (2023) classified sediments into sand versus mud solely based on PFFP penetration depth. Mulukutla et al. (2011) suggested a normalized parameter named firmness factor (which is derived from maximum deceleration, impact velocity, and time of penetration) for classifying the sediments into different grain size classes. These classification schemes focus on specific values of the deceleration curves (such as maximum deceleration) rather than using the full deceleration curves. This leaves information unused and may lead to a higher chance of misclassification. In our study, the full deceleration curve during seabed penetration is considered while using the previous prediction approaches as prior knowledge. Hence, the prediction scheme is divided in two steps:

1. Prediction of sediment class using normalized maximum deceleration and penetration depth
2. Prediction of sediment class using a full and normalized deceleration curve,

where normalized deceleration is defined by (Eq. 1):

$$\text{Normalized Deceleration} = \frac{\text{Deceleration}}{\text{Impact Velocity}} . \quad (1)$$

For the first prediction step, sediment class prediction was performed using a “Random Forest” algorithm, which is a decision tree-based machine learning algorithm. The Random Forest algorithm only uses the normalized maximum deceleration and penetration depth. For the second step, a 1D Bayesian Convolutional Neural Network was applied to the full deceleration curve as an input. Then, these two predictions were combined using a Bayesian approach. Details of each step are discussed in the following sections. A schematic diagram of the proposed predictive model is shown in Figure 4.

Random Forest Model

Random Forest (Breiman 2001), a versatile and powerful ensemble decision tree technique commonly utilized in machine learning, was used to make our initial prediction. It combines the predictive power of multiple decision trees to improve the overall accuracy and robustness of predictions. A decision tree aims to select the best feature at each node to maximize information gain or minimize impurity. In other words, it identifies features that split the data into groups that are as different from each other as possible, or that make the groups as pure and similar as possible. In a Random Forest, a collection of decision trees is constructed, each trained on a random subset of the dataset and with the ability to select a random subset of features for each split. This randomness mitigates overfitting and promotes generalization. In the prediction phase, each tree in the ensemble yields a prediction. These predictions are then combined, either by voting or averaging, to form a single final prediction. This process makes the model more accurate (compared to a single decision tree prediction), and less affected by any irregularities or extreme values in the data. In our case, the normalized maximum deceleration and penetration depth were fed into a Random Forest model

to get a probability estimate of the corresponding sediment classes. The model was implemented using the scikit-learn package (Pedregosa et al. 2011) in python. To train this model, 85% of the whole dataset was used and the rest of the data were kept aside to test the model later.

Bayesian 1D Convolutional Neural Network (CNN)

Neural networks can take in a large number of input variables and have been used extensively in the past in applications related to classification (Krogh 2008). In particular, Convolutional Neural Networks (CNN) have been found to be successful and efficient in the analysis and classification of structured grid data such as images, audio, time series, and text sequences and are commonly used in tasks such as image classification, object detection, and segmentation. For sequential data, such as time series or text, the use of 1D Convolutional Neural Networks (1D CNNs) is generally recommended (Kiranyaz et al. 2021). We adopted a Bayesian variant of CNN, which offers better robustness against over-fitting on small datasets than traditional approaches (Gal and Ghahramani 2016). The model used for this study uses the full seabed penetration deceleration curve and provides the output as uncertainty estimates of each sediment class. A diagram showing the components of the 1D CNN used in this study is shown in Figure 5. In the initial layer of a CNN, the network is traditionally tasked with handling the input sequence. In our specific context, we gather deceleration data at a high frequency of 2 kHz time series (i.e., captured at 0.005-second intervals). However, the size of this input exceeds the number of our sample data which may result in overfitting of the model. To address this, we compute the average deceleration values for every 1 cm of penetration, effectively reducing the input size while preserving the fundamental shape of the deceleration curve. The Convolutional Layers within a CNN play a pivotal role in leveraging learnable filters for local convolutions. In our model, we employ two convolutional layers, each equipped with a specific number of filters. The first convolutional layer is furnished with 32 filters, while the second layer comprises 64 filters. Both layers employ a kernel size of 3, which, in the terminology of 1D CNNs, signifies the length of the filter during convolution. Following the convolutional operation, we apply an activation function elementwise to introduce non-linearity into the neural network. This non-linearity enhances the network's capacity to learn intricate patterns

and increases its expressiveness. In our model, we have chosen the Rectified Linear Unit (ReLU) activation function, as originally proposed by Nair and Hinton (2010). Upon the completion of the two convolutional layers, the output data is flattened into a vector and subsequently fed into fully connected layers. This flattened vector serves as the input for a conventional neural network, establishing connections between every neuron from the preceding layer to every neuron in the subsequent layer. In our model, we have incorporated two hidden layers subsequent to the flattening process. The first hidden layer consists of 1024 neurons, and the second hidden layer comprises 64 neurons. The final layer of the neural network, often referred to as the output layer, is fully connected and contains the same number of neurons as the classes present in the classification task. In our specific case, this number is four. The output layer applies an appropriate activation function to produce the final output probabilities. We have employed the "SoftMax" activation function, a widely recognized choice for multi-class classification, originally introduced by Bridle (1989). In the domain of deep learning, Bayesian Neural Networks offer a distinct probabilistic approach. In contrast, Standard Neural Networks operate deterministically, utilizing fixed model parameters derived from training data to provide point estimates in predictions. While effective, these standard networks are susceptible to overfitting and lack the capability to quantify prediction uncertainty (Goodfellow et al. 2016). Instead, Bayesian Neural Networks treat model parameters as probability distributions. This unique approach equips them with the capacity to provide uncertainty estimates in predictions (Figure 6). Variational inference techniques, commonly applied in Bayesian Neural Networks, approximate these probability distributions, enhancing the robustness of the model and enabling more effective regularization (Graves 2011; Blundell et al. 2015). Bayesian Neural Networks prove particularly advantageous when dealing with limited data and applications that demand a comprehensive understanding of model uncertainty. While doing a prediction, Bayesian Neural Networks sample the model parameters from the trained probability distribution. This is why the model provides a different outcome each time. By creating an ensemble of these different outcomes, we can estimate the uncertainty of the predictions.

Dataset Pre-processing

Prior to inputting the data into the model, it was necessary to perform preprocessing to ensure consistency and suitability for accurate model training. We have gathered a total of 447 samples (pairs of co-located PFFP and sediment sample data). From this dataset, 15% of the samples have been deliberately set aside randomly to form the testing dataset for subsequent evaluation. It's important to note that the testing dataset is comprehensive, containing samples from all four classes. Prior to both the training and testing phases, all data undergoes a scaling process to ensure uniformity and consistency. Despite the overall sample size of 447, our dataset exhibits an inherent class imbalance (see Table 1). Various strategies exist for managing imbalanced datasets, and in our particular case, we have employed the "ADASYN" algorithm, introduced by He et al. (2008). ADASYN stands for "Adaptive Synthetic Sampling" and is an oversampling technique specifically tailored to address imbalanced classification problems. It is essential to emphasize that ADASYN should only be applied to the training dataset to maintain the reliability of validation and testing accuracy metrics. It should not be used in the validation or testing datasets.

Combining Random Forest and 1D Bayesian CNN model

The final task is to combine the predictions obtained from Random Forest and 1D Bayesian CNN model. To do this, the idea of a Bayesian formulation has been applied. The Random Forest model prediction is based on the assumption that the information on the whole deceleration profile can be represented by specific points, such as maximum deceleration, penetration depth, and impact velocity (Jaber and Stark 2023). This idea assumes that the information on the whole deceleration profile can be represented by specific points, such as maximum deceleration, penetration depth, and impact velocity. This assumption simplifies the prediction approach, yet still provides a good approximation of the sediment class. Here, the prediction obtained from the Random Forest model is considered as a *Prior* probability for the 1D Bayesian CNN model. The 1D Bayesian CNN model uses the whole deceleration profile to make a prediction. The algorithm tries to identify differentiating features of the deceleration profile and predict the sediment classes based on the obtained features. This algorithm focuses equally on every part of the deceleration profile which

can reveal additional important information that has been missed by the Random Forest approach. The prediction obtained from this approach can be considered as the likelihood in the Bayesian formulation. By multiplying these two probabilities, we can obtain the final prediction. Since, the probability values of the prior prediction are based on a simple calculation, it can predict zero probability for some classes which can create a problem at the time of multiplication. This zero-probability in the prior will make the final probability zero even if the probability obtained from the second approach is significantly higher than zero. To tackle this issue, the prior probabilities of the four classes are scaled between 0 to 0.6 and then a bias term of 0.1 was added to each class probabilities. These numbers were determined through trial and error to avoid extreme prior probabilities while preserving the overall order of prior probabilities among different classes. This process is illustrated in Figure 7. In this specific example, the obtained probabilities from Random Forest model for class 1, 2, 3 and 4 are 0.8, 0.2, 0.0 and 0.0, respectively. These probability values have been converted to 0.58, 0.22, 0.1 and 0.1 after scaling and adding bias to it. By doing this conversion, we can mitigate extreme prior probability values. As mentioned before, the 1D Bayesian CNN model provides a different probability estimate for the same inputs each time the model is run. Therefore, running the model several times for the same input can create a range of possible probability values for each class. Based on trial and error, it was found that running the model 30-50 times provides stable bounds on the probability of different classes. Figure 8 provides an example of a specific prediction. It displays the predicted uncertainty bounds (Q_1 , Q_2 and Q_3) for class 1 in this prediction after each iteration. This demonstrates that a stable prediction bound can be achieved after 30-50 iterations.

An outline of a step-by-step procedure to obtain predictions of sediment classes is shown in Table 3 with detailed Python code link provided in the data availability section. By following these steps, non-expert users can derive an estimate of sediment behavior classes with their associated uncertainties.

RESULTS AND DISCUSSION

The proposed classification includes uncertainty estimates. Instead of obtaining a single prob-

ability value, the model outputs the range of probability of a given class. Knowledge of the range of probabilities for different outcomes can help users assess the potential risks associated with each prediction. This allows for more informed decision-making.

The confusion matrix for the testing dataset, shown in Figure 9, summarizes how often the classification model incorrectly assigns results from a PFFP drop to a given class. The predicted class label is assigned to the class with highest median probability while the actual class is determined by lab test results. For instance, in the case of class 2, the model accurately predicted 75% of the samples belonging to actual class 2, while misclassifying 25% as class 1. Overall, the model is 91.1% accurate on the test dataset. Examining the misclassifications reveals a consistent pattern: all misclassified instances of Class 1 are erroneously identified as Class 2, and vice versa. A similar pattern emerges for Classes 3 and 4. This observation indicates that the PFFP exhibits distinctly different deceleration curves for cohesionless (Classes 1 and 2) versus cohesive (Classes 3 and 4) sediments, being consistent with previous studies (Mulukutla et al. 2011; Jaber and Stark 2023). However, the distinction becomes less clear between Class 1 and Class 2, as well as between Class 3 and Class 4. The primary differentiator between Classes 1 and 2 is the fines content in the sediment, with a threshold set at 12%. For example, sediments containing 11% and 13% fines may exhibit deceleration curves that are not significantly different, yet they are classified into different categories. Therefore, incorporating an uncertainty estimate is tested to interpret the model results. To elaborate on model's prediction capability, some examples are described herein. Figure 10(a) shows an example of a confident prediction. The result shows that Class 1 (Cohesionless sediment with little to no plasticity) has the highest probability of occurring with this type of deceleration curve with high certainty. This prediction matches the actual lab tested result. Jaber and Stark (2023) suggested that a penetration depth limited to 9 cm indicates sand, also matching our predicted result. For Figure 10(b), the uncertainty estimate shows a large uncertainty between the two cohesionless classes (i.e., Class 1 and 2), but a low chance for cohesive classes (i.e., Class 3 and 4). This indicates that the model is very confident about the fact that it is a cohesionless sediment, but it is not sure whether it belongs to Class 1 or Class 2. A different type of case is presented in

Figure 10(c). For this case, the value of the penetration depth is in an intermediate zone between the value expected for different sediment types. Thus, it is difficult to predict with certainty the class of the sediment. Consistent with this, the proposed model shows large uncertainty (i.e., a spread-out box plot) in the classification. In the case shown in Figure 10(d), we can see the benefits of using the full deceleration profile for prediction. From the traditional approach of PFFP data processing, this deployment was classified as very soft plastic sediment since the penetration depth was close to 80 cm. But this drop clearly looks different than usual PFFP drops, especially in the upper part. Because of this irregularity, the proposed model is showing some probability that it may be Class 1 or 2. This may also indicate the possibility of some other issues, such as layered sediments or biological activity in the area.

The predicted classes have strong potential to be further interpreted to provide approximate sediment behaviors regarding bed erodibility. Erodibility estimates involve calculating critical bed shear stress (τ_{cr}), which is based on sediment properties, indicating sediment strength against hydrodynamic forces (Soulsby, 1997). For cohesionless sediments, τ_{cr} is often estimated by median grain size (d_{50}). With cohesive components, τ_{cr} increases until a mineralogy-dependent threshold, after which it decreases as sediments become fully cohesive (Whitehouse 2000). Applying this to our classification, Class 1 (cohesionless, low plasticity) should have higher erodibility than Class 2 (cohesionless, some plasticity). Shafii et al. (2023) reports a chart for obtaining the range of erodibility based on the USCS classification. According to that chart Class 1 of our classification should fall in "Very High" to "High" erodibility zone and while Class 2 will fall in "High" to "Medium" erodibility zone. Classes 3 (low plastic cohesive) and 4 (high plastic cohesive) exhibit cohesive behavior with significant factors like plasticity, organic content, and biological activity influencing erodibility. Kamphuis and Hall (1983) suggested that with increasing plasticity, the critical bed stress also increases. From this point of view, Class 4 should have lower erodibility than Class 3 if they both had similar fines content since Class 4 has higher plasticity. Both Class 3 and 4 fall within "High" to "Low" erodibility according to Shafii et al. (2023), with variability due to additional factors mentioned above. Sediment transport due to erosion follows three modes:

non-cohesive (bedload), transitional (mix of bedload and suspended load), and cohesive (suspended load). In our classification, Class 1 should align with non-cohesive to transitional modes, Class 2 with transitional to cohesive modes, and Classes 3 and 4 with cohesive sediment transport.

Another sediment behavior that the predicted classes can provide insight into is susceptibility to wave-induced liquefaction, which significantly depends on sediment composition. Under large, steep waves in relatively shallow water, high permeability, clean sands containing small amounts of gas can be prone to momentary wave-induced liquefaction because the gas causes the pore water-gas mixture to become compressible (Michallet et al. 2009). Under less extreme wave conditions, residual liquefaction can occur in semi-permeable sand-mud mixtures due to the build-up of excess pore pressure over a series of waves. Experiments with kaolinite-fine sand mixtures and illite-fine sand mixtures demonstrated that low but non-zero clay content ($\geq 0.5\%$) increases susceptibility to residual liquefaction in semi-permeable, loosely compacted sands, while higher clay content (typically over 10-30%, depending on clay minerals) can decrease susceptibility as permeability and compressibility decrease (Zhang et al. 2020). This suggests that Class 1 may be the only class susceptible to momentary wave-induced liquefaction, while Classes 1 and 2 sediments may be prone to wave-induced residual liquefaction to differing degrees, depending on their compaction and fines content. Predominantly fine-grained classes (Class 3 and 4) may be minimally susceptible to wave-induced liquefaction because their permeability is too low.

Object burial is an additional important process that researchers work to predict using sediment behavior. It is a complex process influenced by bearing failure, scouring, consolidation, and fluidization. Scour burial within fully cohesionless sediments (Class 1) has been well-documented (Traykovski et al. 2007; Trembanis et al. 2007; Whitehouse 1998). Friedrichs et al. (2016) found that, acting alone, scour burial is typically limited to lowering the base of the object to 1 to 1.5 diameters below the far-field seabed surface in cohesionless sediments (Class 1 and Class 2). At that point, the action of scour simply keeps the object from being fully covered. Conversely, cohesive sediments (Class 3 and 4) tend to exhibit notably higher burial depths due to impact burial followed by consolidation (Trembanis and DuVal 2021). Overall, due to the combined effects of

scour, impact, and consolidation burial, objects in Class 1 and Class 2 sediments should often be partially exposed, while Class 3 and Class 4 sediments should more typically be fully buried.

The uncertainty estimates from the proposed model can be further interpreted to reveal insights into sediment behaviors. For instance, the sediment depicted in Figure 10(b) is likely Class 1 or Class 2. As discussed earlier, this suggests that the sediment will have "Very High" to "Medium" erodibility, as approximated by Shafii et al. (2023). Factors such as plasticity, organic content, and biological activity will be less significant to sediment properties since these become relatively more important in fine-grained cohesive sediments (Class 3 and 4).

The methodology presented in this paper takes a different approach from (Jaber and Stark 2023) for interpreting PFFP data. Instead of predicting specific geotechnical properties, such as undrained shear strength or friction angle, it classifies the deceleration curve obtained from PFFP and assigns sediment behavior types based on that classification. This method avoids imposing assumptions on empirical parameters such as the cone factor and strain rate correction factor, making the interpretation of PFFP data more user-friendly, especially for users without a geotechnical engineering background.

A key question about this study is whether the model can be applied to other sites, especially those with different sediment characteristics than the training data, since data from only three main locations have been used. If the input deceleration curve is very different from what the model was trained on, the model will show a higher degree of uncertainty in its predictions. This uncertainty, known as epistemic uncertainty (Der Kiureghian and Ditlevsen 2009), happens because the model lacks enough data to make accurate predictions for these new conditions. By adding more data to the training set, this uncertainty can be reduced, which eventually will make the model more accurate. The model is designed to easily incorporate additional data, which means it can be improved and become more reliable for a wider range of conditions in the future.

CONCLUSION

This study introduces a novel predictive model for classifying sediment behavior using data from Portable Free Fall Penetrometer (PFFP) deployments. By integrating Random Forest and

1D Bayesian Convolutional Neural Network algorithms, the model is capable of high accuracy and reliability in sediment classification. The four sediment classes identified offer valuable insights into sediment characteristics essential for coastal engineering applications. The model not only categorizes sediments but also provides uncertainty estimates, offering a probabilistic range for each class prediction. This enhances decision-making processes by allowing users to assess potential risks and interpret sediment behavior more comprehensively. Importantly, the model avoids assumptions about parameters such as the cone factor and strain rate correction factor, making it accessible to those without specialized geotechnical expertise.

However, the study acknowledges limitations, particularly the reliance on PFFP measurements from only three locations for training and testing the model, which raises concerns about its generalizability. Nevertheless, the model's design allows for the incorporation of additional data, suggesting that expanding the training dataset with more diverse sites and environmental conditions could significantly enhance its applicability. Future research should focus on expanding the dataset and refining the model to improve its robustness and accuracy further. Exploring quantitative approaches for predicting erodibility or object burial using the full potential of PFFP datasets could also be beneficial. Such advancements would greatly enhance sediment mapping processes and engineering decision-making in nearshore environments, ultimately contributing to more effective coastal management and infrastructure development.

ACKNOWLEDGEMENT

Funding for this work was provided by the Strategic Environmental Research and Development Program (SERDP) through grant MR21-1265. The authors thank Eric Hunstein, Saurav Shrestha, Elise Hummel, Nick Brill, and Jonathan Moore (all from Virginia Tech) and Chesna Cox (DISL) for their assistance with field measurements.

DATA AVAILABILITY STATEMENT

Some or all data, models, or code generated or used during the study are available in a repository online in accordance with funder data retention policies. https://github.com/Rejwan05/PFFP_Prediction.git

List of Tables

1	Distribution of PFFP dataset among different locations	18
2	Gradation and plasticity criteria for sediment behavior types used in this study . . .	18
3	Step-by-step procedure to obtain sediment behavior classes from PFFP data	19

List of Figures

1	(a) Deployment of PFFP (b) Displacement vs deceleration/velocity plot of PFFP from point of release to stop (c) Zoomed in version of (b) showing seabed penetration only	20
2	PFFP deployment locations. (a) Sequim Bay, (b) Potomac River, (c) York River, and (d) overview map	21
3	PFFP data used for training and testing of the predictive model displayed with regards to the maximum deceleration recorded by the PFFP, the PFFP penetration depth, and the assigned sediment classes based on laboratory testing of sediment samples	22
4	Schematic diagram of the proposed predictive model	22
5	Neural network architecture with 211-feature input layer, 1D convolutional layers for feature extraction, fully connected layers for flattening the extracted features, and 4-neuron output layer for sediment classification	23
6	Basic difference between standard and Bayesian neural networks. The weights in the standard neural network are specific values whereas in the Bayesian neural network the weights are in form of probability distributions	23
7	Modification process of probability values obtained from random forest model to eliminate extreme priors. (a) Probability obtained from random forest model. (b) Scaled probability within 0.0-0.6 range (c) Modified probability after adding bias term to the scaled probability	24

8	An example prediction of the model indicating the uncertainty bounds Q_1 , Q_2 and Q_3 for class 1. (b) Change of uncertainty bounds Q_1 , Q_2 and Q_3 with number of iterations	24
9	Confusion matrix for testing dataset. The percentage values on the right diagonal (shown in green) represent the percentage of times the predicted value matched the actual values for each class.	25
10	Different types of prediction cases obtained from the proposed model. (a) prediction case showing little to no uncertainty in prediction. (b) Prediction case showing uncertainty between two cohesionless classes. (c) Prediction case showing uncertainty among three classes. (d) Prediction case for a deceleration curve likely affected by shell hash and clams	26

TABLE 1. Distribution of PFFP dataset among different locations

Location (1)	Sub-location (2)	Number of PFFP Deployments (3)
York River, VA	Clay Bank	126
	Pamunkey	45
	Naval Weapon Station	25
	Ferry Point	21
	Sarah's Creek	28
	Coast Guard	25
	York Mouth	15
	Goodwin Island	27
Potomac River, VA		72
Sequim Bay, WA		63
Total		447

TABLE 2. Gradation and plasticity criteria for sediment behavior types used in this study

Class No. (1)	Sediment Behavior Types (2)	Corresponding USCS Class* (3)	Dataset Size (4)
1	Cohesionless Sediment with Little to No Plasticity: Sand Content > 50% & Fines Content < 12%	SP, SW, SP-SM, SP-SC, SW-SM, SW-SC	92
2	Cohesionless Sediment with Some Plasticity: Sand Content > 50% & Fines Content > 12%	SM, SC, SC-SM	65
3	Cohesive Sediment with Low Plasticity: Fines Content > 50% & Liquid Limit < 50%	ML, CL, CL-ML	23
4	Cohesive Sediment with High Plasticity: Fines Content > 50% & Liquid Limit > 50%	MH, CH	267

*Description of soil types for different USCS symbols:

SP = Poorly graded sand, SW = Well-graded sand, SM = Silty sand, SC = Clayey sand,

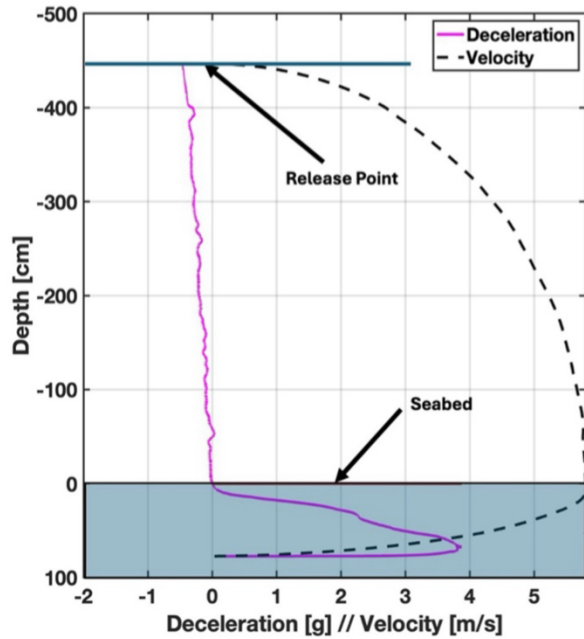
ML = Low-plastic silt, CL = Low-plastic clay, MH = High-plastic silt, CH = High-plastic clay

TABLE 3. Step-by-step procedure to obtain sediment behavior classes from PFFP data

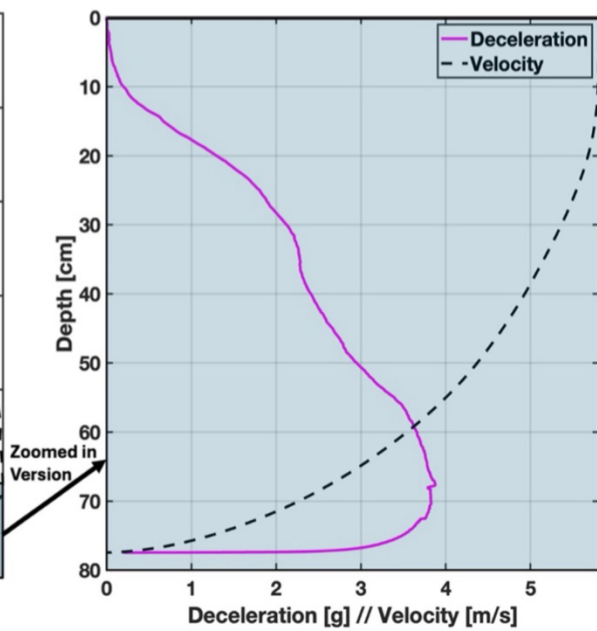
Step	Task Performed in the Step
(1)	(2)
1	Obtain the Deceleration profile from the start of penetrating the sediment. Integrate it with time to obtain the velocity profile and penetration depth.
2	Determine the impact velocity and obtain the Normalized Deceleration Profile by using (1).
3	Take the Normalized Maximum Deceleration and Penetration Depth and feed it into the Random Forest model to obtain the prior probability estimate for each sediment class.
4	Take the Normalized Deceleration profile and extract the values at 1 cm depth intervals. Then feed the decimated profile into the 1D Bayesian CNN model to obtain the likelihood probabilities for each class.
5	Multiply each of the likelihood probabilities (Step 4) with the scaled prior probabilities (Step 3). Normalize the probability values so that the summation of probability of four classes becomes 1.
6	Repeat Steps 4 and 5, 30 to 50 times with the same input deceleration profile. The model should provide different probability outputs for each run. Thus, it will provide a range of probabilities for each class.
7	Plot the values and create a box plot for better visualization.



(a)



(b)



(c)

Fig. 1. (a) Deployment of PFFP (b) Displacement vs deceleration/velocity plot of PFFP from point of release to stop (c) Zoomed in version of (b) showing seabed penetration only

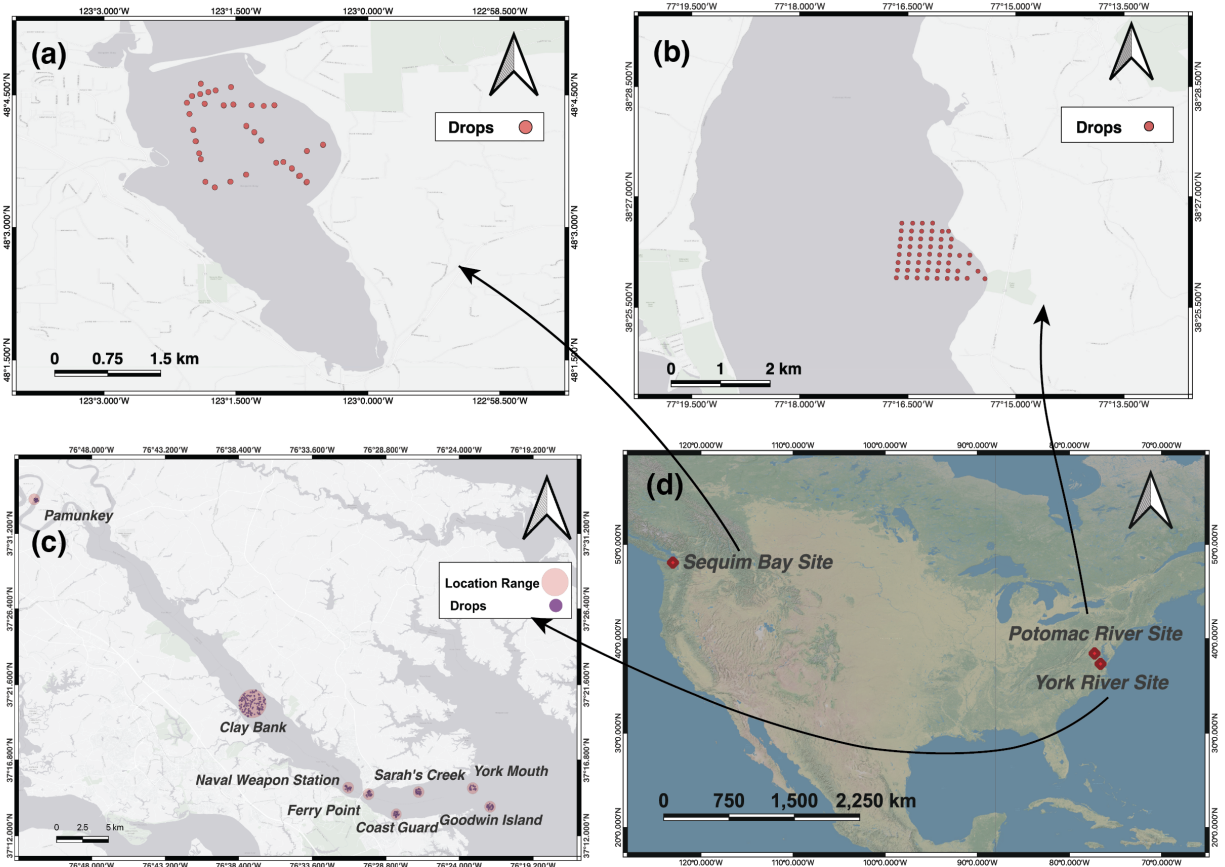


Fig. 2. PFFP deployment locations. (a) Sequim Bay, (b) Potomac River, (c) York River, and (d) overview map

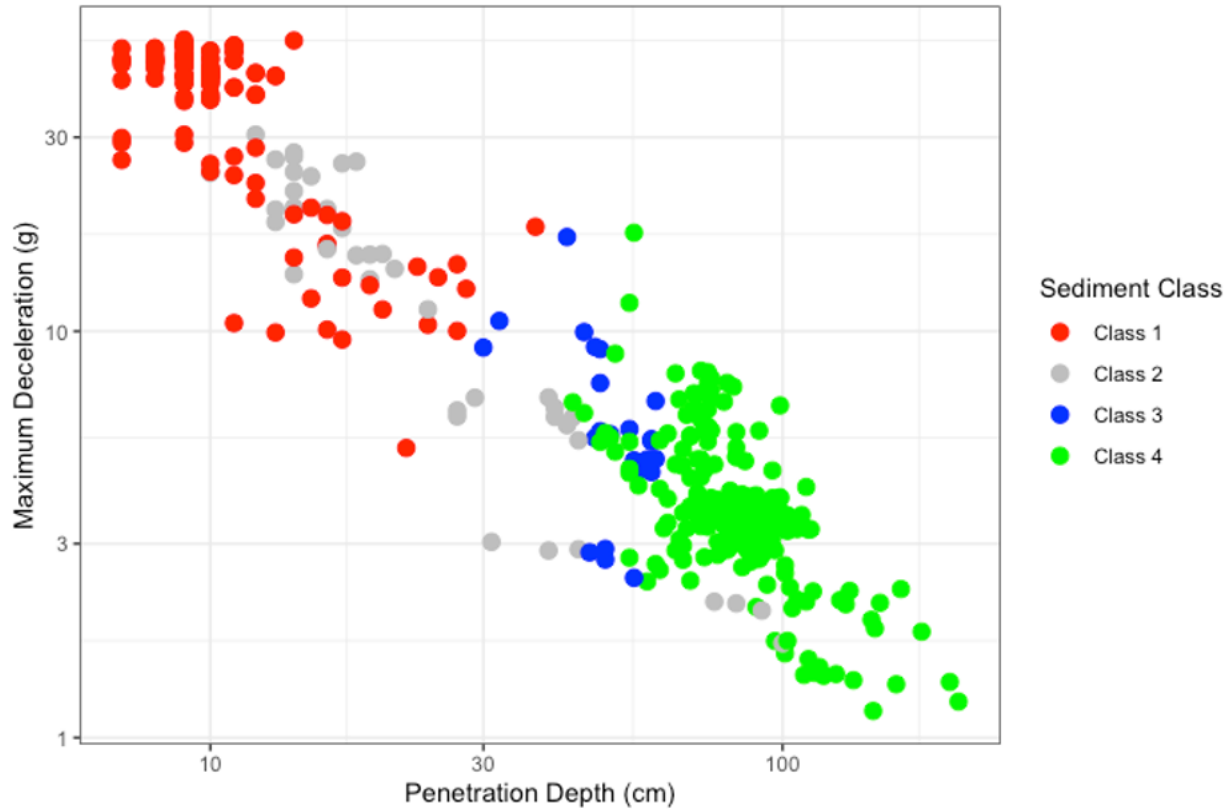


Fig. 3. PFFP data used for training and testing of the predictive model displayed with regards to the maximum deceleration recorded by the PFFP, the PFFP penetration depth, and the assigned sediment classes based on laboratory testing of sediment samples

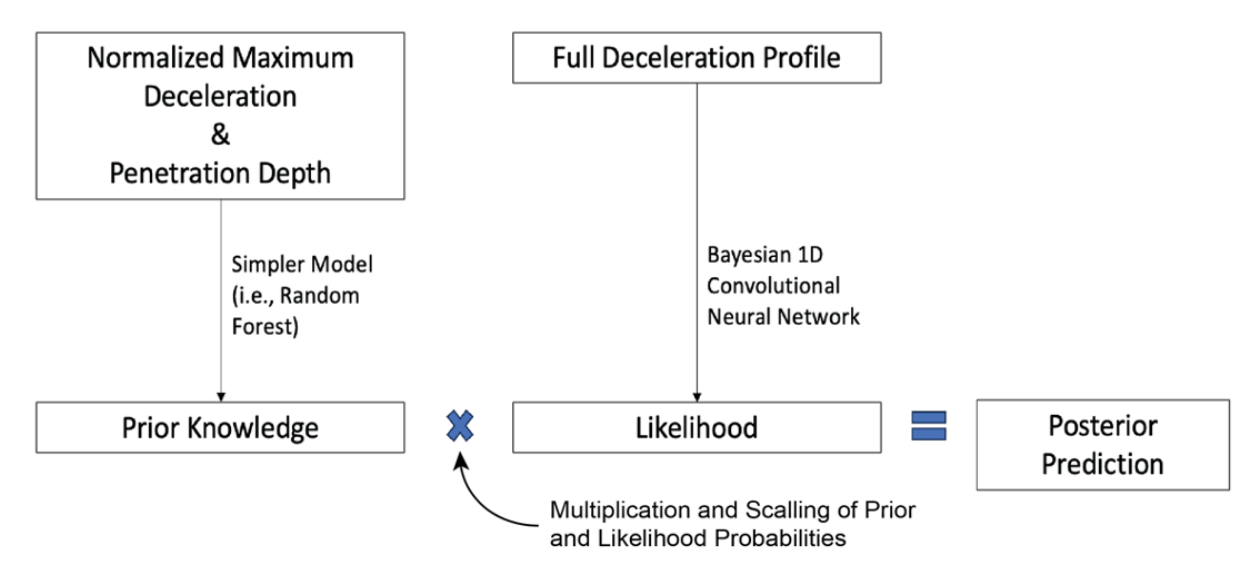


Fig. 4. Schematic diagram of the proposed predictive model

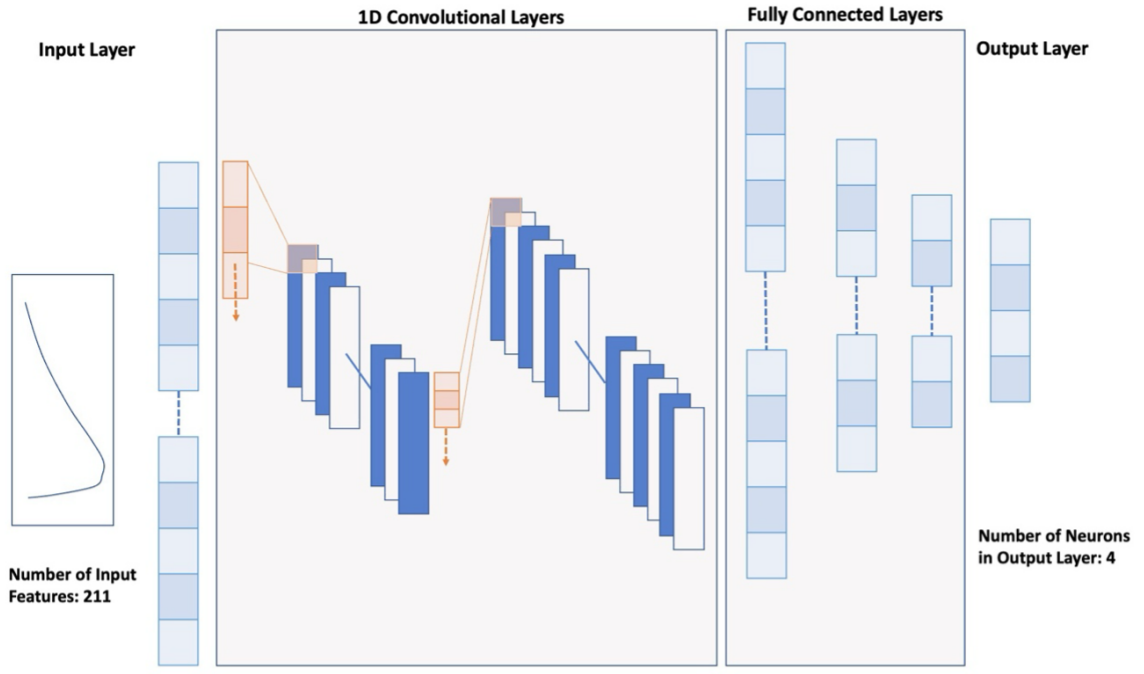


Fig. 5. Neural network architecture with 211-feature input layer, 1D convolutional layers for feature extraction, fully connected layers for flattening the extracted features, and 4-neuron output layer for sediment classification

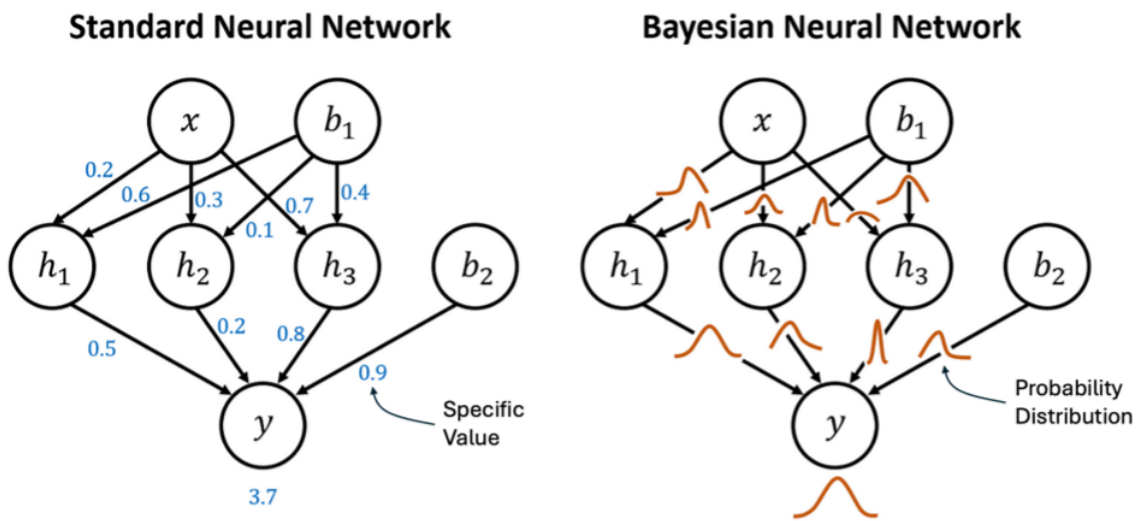


Fig. 6. Basic difference between standard and Bayesian neural networks. The weights in the standard neural network are specific values whereas in the Bayesian neural network the weights are in form of probability distributions

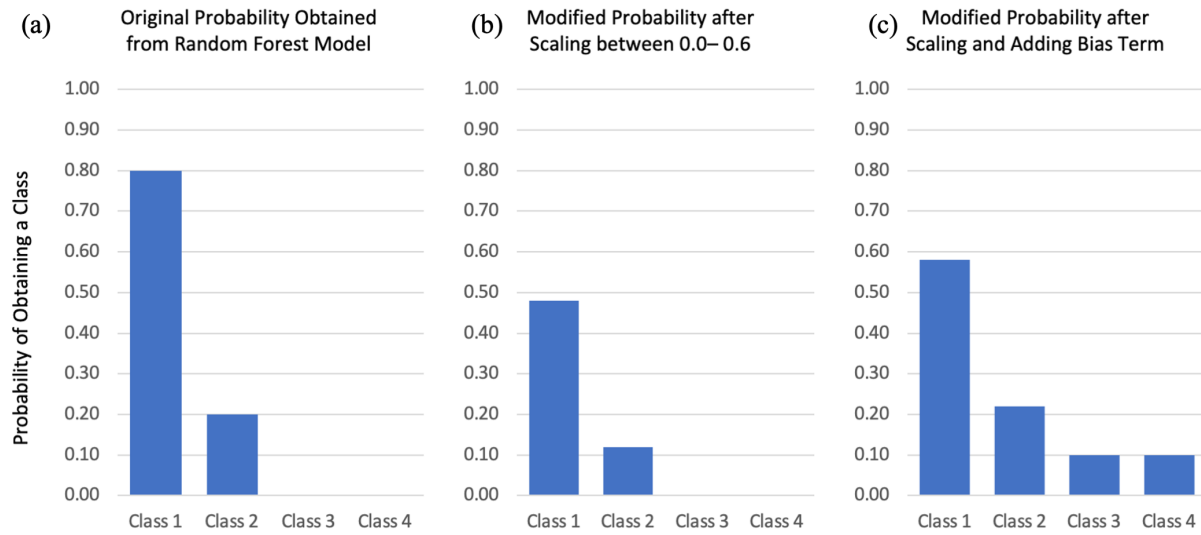


Fig. 7. Modification process of probability values obtained from random forest model to eliminate extreme priors. (a) Probability obtained from random forest model. (b) Scaled probability within 0.0-0.6 range (c) Modified probability after adding bias term to the scaled probability

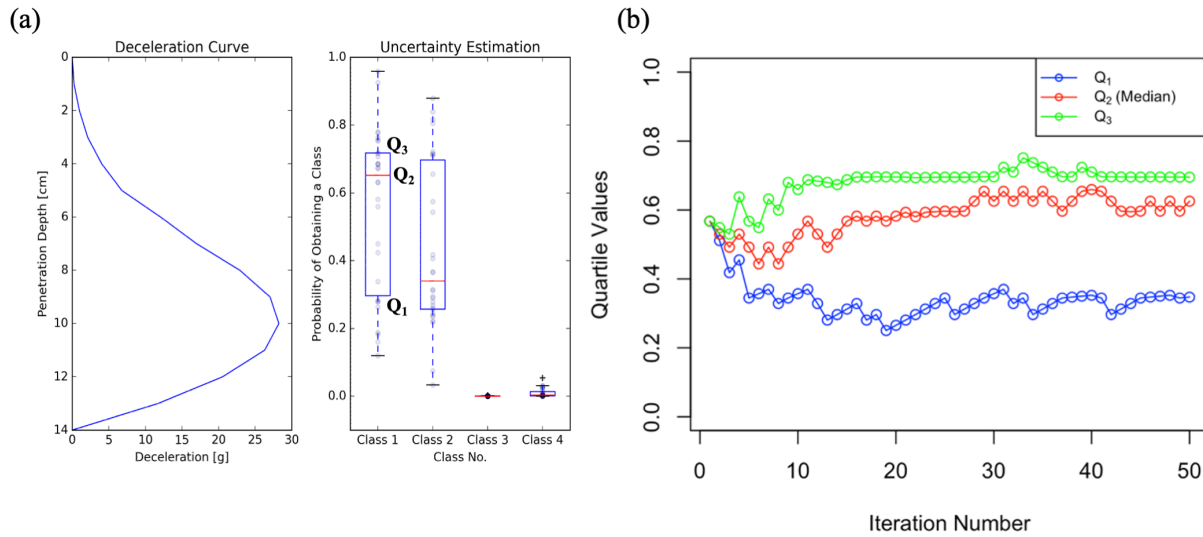


Fig. 8. An example prediction of the model indicating the uncertainty bounds Q_1 , Q_2 and Q_3 for class 1. (b) Change of uncertainty bounds Q_1 , Q_2 and Q_3 with number of iterations



Fig. 9. Confusion matrix for testing dataset. The percentage values on the right diagonal (shown in green) represent the percentage of times the predicted value matched the actual values for each class.

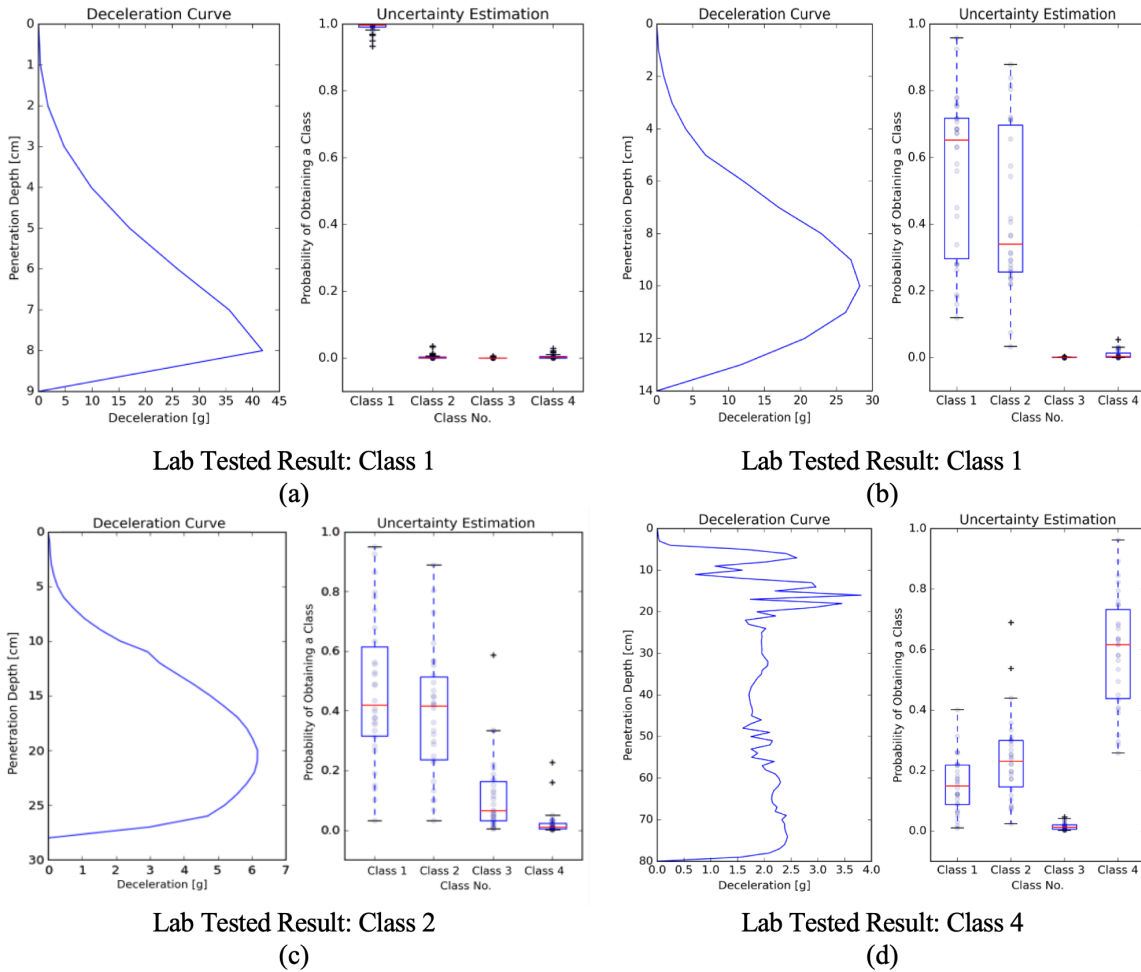


Fig. 10. Different types of prediction cases obtained from the proposed model. (a) prediction case showing little to no uncertainty in prediction. (b) Prediction case showing uncertainty between two cohesionless classes. (c) Prediction case showing uncertainty among three classes. (d) Prediction case for a deceleration curve likely affected by shell hash and clams

REFERENCES

- Akal, T. and Stoll, R. (1995). "An expendable penetrometer for rapid assessment of seafloor parameters." *'Challenges of Our Changing Global Environment'. Conference Proceedings. OCEANS'95 MTS/IEEE*, Vol. 3, IEEE, 1822–1826.
- Albatal, A. and Stark, N. (2017). "Rapid sediment mapping and in situ geotechnical characterization in challenging aquatic areas." *Limnology and Oceanography: Methods*, 15(8), 690–705.
- Albatal, A., Stark, N., and Castellanos, B. (2020). "Estimating in situ relative density and friction

- angle of nearshore sand from portable free-fall penetrometer tests.” *Canadian Geotechnical Journal*, 57(1), 17–31.
- ASTM (2017). *Standard Practice for Classification of Soils for Engineering Purposes (Unified Soil Classification System)*. ASTM D2487-17, West Conshohocken, PA.
- Aubeny, C. and Shi, H. (2006). “Interpretation of impact penetration measurements in soft clays.” *Journal of Geotechnical and Geoenvironmental Engineering*, 133(7), 767–781.
- Bilici, C., Stark, N., Friedrichs, C., and Massey, G. (2019). “Coupled sedimentological and geotechnical data analysis of surficial sediment layer characteristics in a tidal estuary.” *Geo-Marine Letters*, 39(3), 175–189.
- Blundell, C., Cornebise, J., Kavukcuoglu, K., and Wierstra, D. (2015). “Weight uncertainty in neural network.” *International conference on machine learning*, PMLR, 1613–1622.
- Breiman, L. (2001). “Random forests.” *Machine learning*, 45, 5–32.
- Bridle, J. (1989). “Training stochastic model recognition algorithms as networks can lead to maximum mutual information estimation of parameters.” *Advances in neural information processing systems*, Vol. 2.
- Cetin, K. and Ozan, C. (2009). “Cpt-based probabilistic soil characterization and classification.” *Journal of Geotechnical and Geoenvironmental Engineering*, 135(1), 84–107.
- Chow, S., O’Loughlin, C., and Randolph, M. (2014). “Soil strength estimation and pore pressure dissipation for free-fall piezocone in soft clay.” *Géotechnique*, 64, 817–827.
- Chow, S., O’Loughlin, C., White, D., and Randolph, M. (2017). “An extended interpretation of the free-fall piezocone test in clay.” *Géotechnique*, 67(12), 1090–1103.
- Der Kiureghian, A. and Ditlevsen, O. (2009). “Aleatory or epistemic? does it matter?.” *Structural safety*, 31(2), 105–112.
- Friedrichs, C., Rennie, S., and Brandt, A. (2016). “Self-burial of objects on sandy beds by scour: A synthesis of observations.” *Scour and Erosion: Proceedings of the 8th International Conference on Scour and Erosion*, CRC Press, 179.
- Gal, Y. and Ghahramani, Z. (2016). “Bayesian convolutional neural networks with bernoulli approx-

- imate variational inference.” *4th International Conference on Learning Representations (ICLR) workshop track*.
- Goodfellow, I., Bengio, Y., and Courville, A. (2016). *Deep learning*. MIT press.
- Graves, A. (2011). “Practical variational inference for neural networks.” *Advances in neural information processing systems*, Vol. 24.
- He, H., Bai, Y., Garcia, E., and Li, S. (2008). “Adasyn: Adaptive synthetic sampling approach for imbalanced learning.” *2008 IEEE international joint conference on neural networks (IEEE world congress on computational intelligence)*, 1322–1328.
- Hunstein, E., Stark, N., and Rodriguez-Marek, A. (2023). “Finding the mudline: Automatization of seabed impact selection for a portable free-fall penetrometer.” *Journal of Geotechnical and Geoenvironmental Engineering*, 149(12), 06023008.
- Jaber, R. and Stark, N. (2023). “Geotechnical properties from portable free fall penetrometer measurements in coastal environments.” *Journal of Geotechnical and Geoenvironmental Engineering*, 149(12), 04023120.
- Jung, B., Gardoni, P., and Biscontin, A. (2008). “Probabilistic soil identification based on cone penetration tests.” *Géotechnique*, 58(7), 591–603.
- Kamphuis, J. and Hall, K. (1983). “Cohesive material erosion by unidirectional current.” *Journal of Hydraulic Engineering*, 109(1), 49–61.
- Kiranyaz, S., Avci, O., Abdeljaber, O., Ince, T., Gabbouj, M., and Inman, D. (2021). “1d convolutional neural networks and applications: A survey.” *Mechanical Systems and Signal Processing*, 151, 107398.
- Krogh, A. (2008). “What are artificial neural networks?.” *Nature Biotechnology*, 26(2), 195–197.
- Michallet, H., Mory, M., and Piedra-Cueva, I. (2009). “Wave-induced pore pressure measurements near a coastal structure.” *Journal of Geophysical Research: Oceans*, 114(C6).
- Mulukutla, G., Huff, L., Melton, J., Baldwin, K., and Mayer, L. (2011). “Sediment identification using free fall penetrometer acceleration-time histories.” *Marine Geophysical Research*, 32, 397–411.

- Mumtaz, B., Stark, N., and Brizzolara, S. (2018). "Pore pressure measurements using a portable free fall penetrometer." *Proc. Cone Penetration Testing 2018 (CPT'18)*, London, CRC Press.
- Nair, V. and Hinton, G. (2010). "Rectified linear units improve restricted boltzmann machines." *Proceedings of the 27th International Conference on Machine Learning*, 807–814.
- Olsen, R. and Mitchell, J. (1995). "Cpt stress normalization and prediction of soil classification." *Proceedings of the International Symposium on Cone Penetration Testing, CPT'95*, Vol. 2, 257–262.
- Pedregosa, F., Varoquaux, G., Gramfort, A., Michel, V., Thirion, B., Grisel, O., Blondel, M., Prettenhofer, P., Weiss, R., Dubourg, V., Vanderplas, J., Passos, A., Cournapeau, D., Brucher, M., Perrot, M., and Duchesnay, E. (2011). "Scikit-learn: Machine learning in python." *Journal of Machine Learning Research*, 12, 2825–2830.
- Robertson, P. (1990). "Soil classification using the cpt." *Canadian Geotechnical Journal*, 27(1), 151–158.
- Shafii, I., Medina-Cetina, Z., Shidlovskaya, A., and Briaud, J.-L. (2023). "Relationship between soil erodibility and soil properties." *Journal of Geotechnical and Geoenvironmental Engineering*, 149(1), 04022121.
- Stark, N., Coco, G., Bryan, K. R., and Kopf, A. (2012). "In-situ geotechnical characterization of mixed-grain-size bedforms using a dynamic penetrometer." *Journal of Sedimentary Research*, 82(7), 540–544.
- Traykovski, P., Richardson, M., Mayer, L., and Irish, J. (2007). "Mine burial experiments at the martha's vineyard coastal observatory." *IEEE Journal of Oceanic Engineering*, 32(1), 150–160.
- Trembanis, A. and DuVal, C. (2021). "Further examining the role of cohesive sediments in munitions mobility through additional infield deployment of smart munitions and application of a serdp-developed penetrometer.
- Trembanis, A., Friedrichs, C., Richardson, M., Traykovski, P., Howd, P., Elmore, P., and Wever, T. (2007). "Predicting seabed burial of cylinders by wave-induced scour: Application to the sandy inner shelf off florida and massachusetts." *IEEE Journal of Oceanic Engineering*, 32(1),

167–183.

Whitehouse, R. (1998). *Scour at marine structures: A manual for practical applications*. Thomas Telford.

Whitehouse, R. (2000). *Dynamics of estuarine muds: a manual for practical applications*. Thomas Telford.

Zhang, J., Jiang, Q., Jeng, D., Zhang, C., Chen, X., and Wang, L. (2020). “Experimental study on mechanism of wave-induced liquefaction of sand-clay seabed.” *Journal of Marine Science and Engineering*, 8(2), 66.